

Sustainable Bioactivity Enhancement of Ag/ZnO Nanoparticles in Antimicrobial Applications

Sara S. Hamood¹, Majid S. Khalaf¹, Firas S. Mohammed²

¹Department of physics, College of Science, Mustansiriyah University, Baghdad, Iraq.

² Ministry of Science and Technology, Directorate of Treatment of Military, Biological, and Chemical Disposal, Baghdad, Iraq.

Corresponding Author: E-mail: sarasameer@uomustansiriyah.edu.iq

Keywords:

Zinc oxide nanoparticles, silver nanoparticles, pulsed laser ablation, antibacterial.

Abstract

Due to their unique characteristics, zinc oxide nanoparticles (ZnO NPs) are well suited for usage in a range of fields, including medicine and environment. In this study, ZnO, Ag, and mixed (Ag/ZnO) nanoparticles were produced by using the pulsed laser ablation method, which is one of the most popular and straightforward techniques to make these compounds since it produces nanoparticles with a high bioavailability and low toxicity. A variety of analysis, such as XRD, UV-vis, TEM and Antibacterial were employed to assess and describe the Nano-products. Additionally, these nanoparticles were used in an antibacterial activity against several microorganisms. The results illustrated the normal behavior of these nanoparticles. Comparisons were made among the products.

Introduction

The unique optical, electrical, and magnetic characteristics of semiconductor nanoparticles (NPs) and the applications for which they are used are particularly significant. By reducing the size dimension to the atomic level, NPs' characteristics alter [1]. One of them is ZnO nanoparticle, which is thought to be one of the most cutting-edge and encouraging materials since its high direct bandgap plus its significant binding energy of exciton (60 meV) at 25 C° [2-5]. ZnO NPs are used extensively in photonics, array sensors, and catalysts [6, 7]. However, the practical uses of ZnO were determined though their characteristics that may change via altering its shape [8]. Another metal substance that has been studied extensively is silver nanoparticles (AgNPs) which can be used as an alternative to antibiotics to suppress or eliminate bacteria [9–12]. Thus, investigators attempted to use multiple techniques such as Radiofrequency sputtering [13], physical evaporation [14], colloidal fabrication process [15], thermal treatment [16], electrodeposition [17], precipitate [18-21] ...etc. The Puls-Laser

Ablation approach has recently been demonstrated to be an efficient way to manufacture various substances at the nanoscale [22]. The advantages of the PLA Method include the ability to produce well-crystallized nanoparticles that are clean and free of by-products, low-cost tools for controlling the ablation, additionally, capability of controlling the surface to volume ratio for created material by adjusting a variety of variables, including laser fluency, pulse laser duration, laser wavelength, changing the solution's temperature or pH, and introducing surfactants as well [23-26].

Experimental procedure

1- Synthesis of Ag/ZnO nanoparticles by the PLA Method:

Synthesizing of Zinc Oxide and Silver individually plus the tagged ZnO:Ag NPs were by using PLAL method to in deionized water. Figure (1) shows the experimental configuration in detail. The plate of approximately pure metal (>99.99%) had been put in a glass vessel containing 1.5 milliliter of DIW. A Neodymium-Yag laser that has a specification (wavelength 1064 nm with a repetition rate of 2 Hz and 420 mJ/pulse) was then used to ablate the material. A hundred millimeters converging lens has been employed for concentrating the beam of laser onto the metal plate. The ZnO:Ag nanostructures were created using a two-step process. First, a glass jar has been placed with a 2-mm-thick silver plate positioned on the bottom, and it is positioned 1 cm away from the top surface. It took 60 minutes to continually ablate the silver plate. In order to create ZnO:Ag NPs, same laser having same power abated a zinc plate for one hour in the Ag nano particles suspended in the solution that was created in the pre stage.

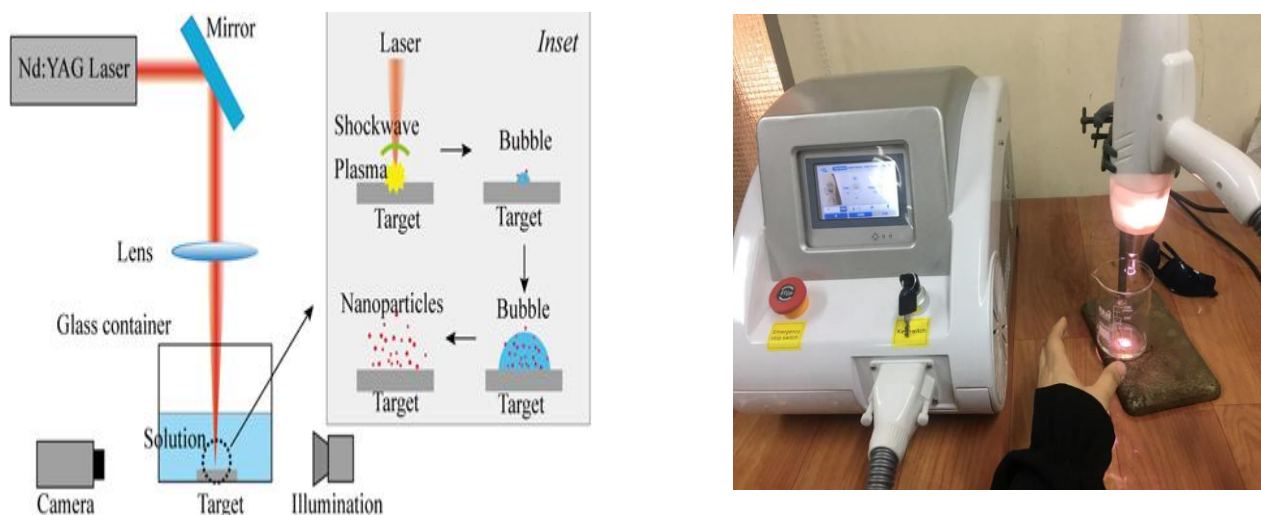


Figure 1: (a) Schematic diagram of the PLAL setup and (b) real image for the PLAL setup.

2- Antibacterial activity

Antibacterial activity was done for all samples synthesis by laser ablation methods, against two bacterial species for thick and thin peptidoglycan (*S.aureus*) and only thin peptidoglycan (*E-coli*). The microbial cultures were provided by the antibacterial activity laboratory /Department of Biology / College of Sciences/ Mustansiriyah University. Agar well diffusion techniques were used to conduct the experiment in sterile petri dishes with a 90 mm diameter that contained sterile nutritional agar media. At 25 °C, the pH was corrected to 6.8. Following that, MONPs were created using two different techniques and then dissolved in DIW, a solvent with a concentration of (40 mg/mL). The petri-dish surface was swabbed with the freshly created microorganisms. Each plate's bacterial media was divided into six 6-mm-diameter wells using a sterile gel puncher/crok borer. For the two-technique synthesis, a control (DIW) for two different types of bacteria is added into each well, which includes (40 L) of MONPs NPs. The test samples were incubated at ± 25 °C for one day for bacteria followed by scaling the diameter of inhibition in (mm). The formula below was employed to measure the percentage of inhibition [27].

$$\text{Inhibition zone}(\%) = \frac{\text{Diameter of the inhibition zone}}{\text{Diameter of the petriplate}(90\text{mm})} \times 100 \dots \dots \dots (1)$$

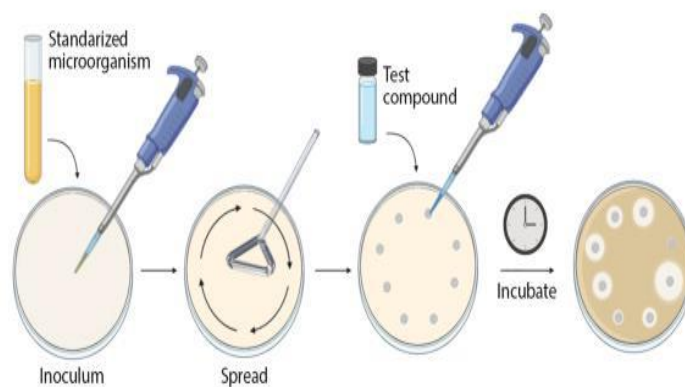


Figure 2: Scheme of the agar disk diffusion method

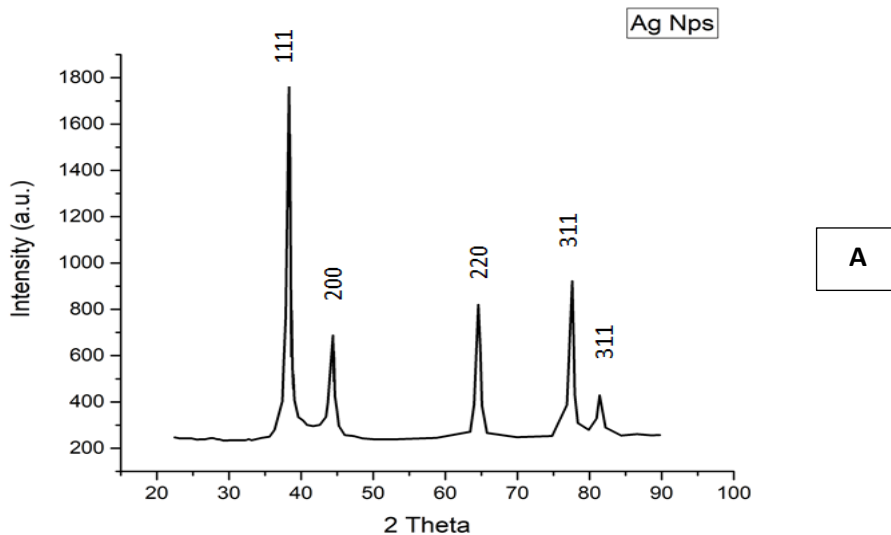
Results and discussion

1- X-ray patterns of nanoparticles

figure (3), was used to determine the phases and crystallographic composition. The XRD structure of Ag NPs is depicted by the black curve illustrated in figure (3A). It is demonstrated that the crystalline planes of Ag NPs at the 2 values of 38.3° , 45.50° , 64.1° , and 78.1° correspond to (111), (200), (220), and (311) of silver nanoparticle correspondingly. The data on Diffraction Standards (JCPDS) file

showing Ag have a face-centered cubic which agrees with these peaks. Six peaks can be found at 31.5°, 34.18°, 36.02°, 42.34°, 46.34°, and 52.7° on the black curve in figure (3B), which is ascribed to the crystalline planes of (100), (002), (101), (102), (110), and (103) of Zinc Oxide NPs, correspondingly. According to JCPDS card number 36-1451, all of these ZnO NP XRD peaks were identified to the hexagonal wurzite structure of ZnO [28]. The findings demonstrate the high crystal purity of the ZnO NPs. The XRD pattern of the ZnO:Ag nanostructure is represented by the red line in figure (3B). The face-centered framework of Ag (JCPDS card no. 04-0783) and the hexagonal wurzite configuration of Zinc Oxide (JCPDS card no. 36-1451) are discovered to match to two sets of diffraction peaks. No discernible change through pattern peak values of Silver and Zinc Oxide in relation to the diffraction peaks in Silver and Zinc Oxide nanoparticle. The presence of Ag nanoparticles and the lack of other impurity diffraction peaks point to the great purity of the ZnO:Ag nanostructure produced using ablated laser. The crystallinity of the composites, the average crystallite size of mostly NPs was calculated using the Debye-Scherrer equation after successful synthesis. The Scherrer equation is the basic and most widely used equation for calculating crystallite size by combining 2θ and FWHM values from XRD data, as shown in the table (1).

$$D = \frac{K\lambda}{\beta} \cos\theta \dots \dots \dots (2)$$



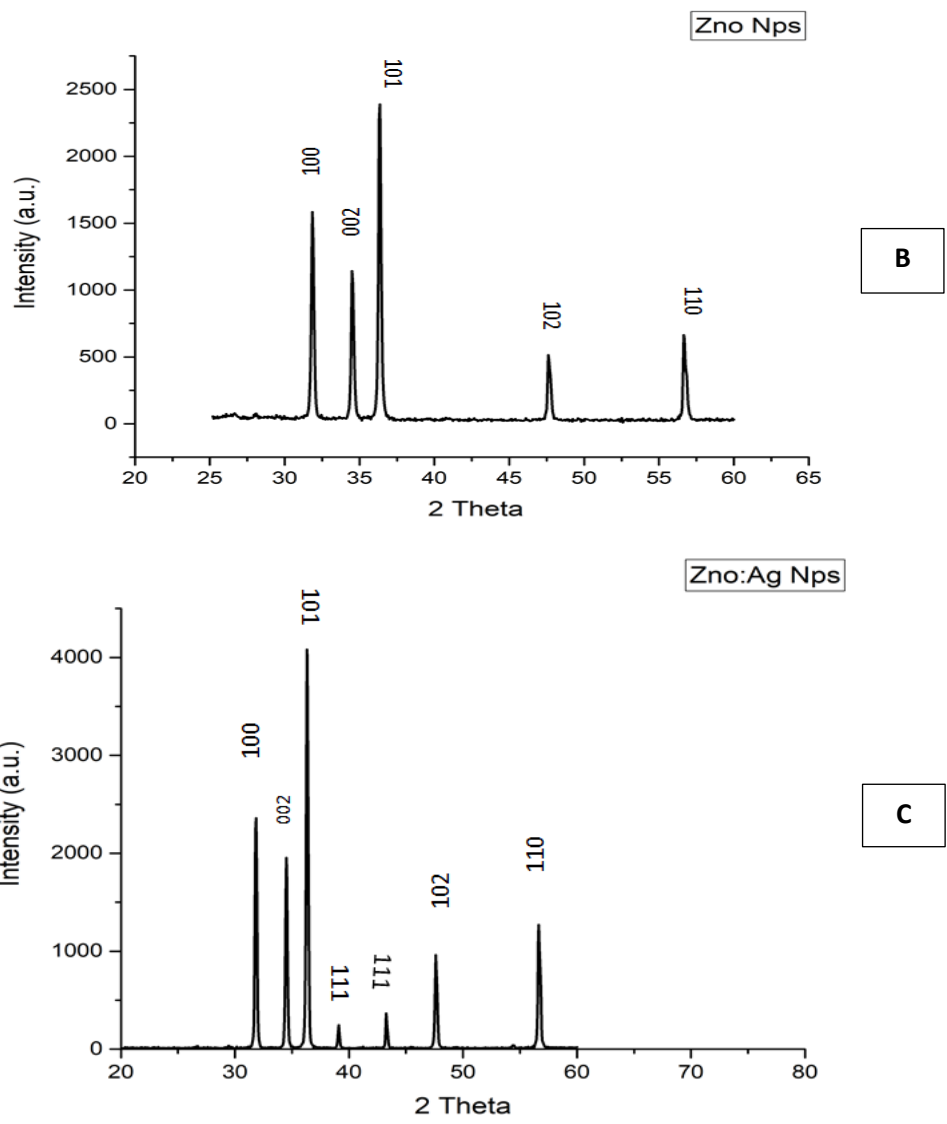


Figure 3: XRD Patterns of (a) Zinc oxide,(b) silver and (c) Ag/ZnO Nanoparticles.

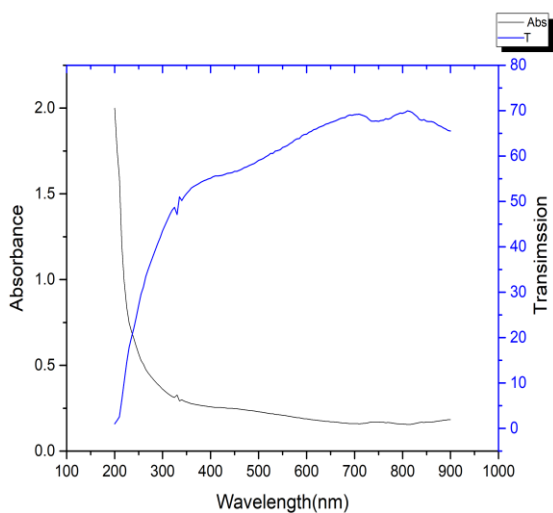
Table (1) XRD parameters of Zinc oxide and ZnO:Ag Nanoparticles.

ZnO NPs			
2θ(Degree)	(hkl)	d(nm)	FWHM
11.68871		1.678693	4.7553
20.4745	100	1.032773	7.81359
29.55008	002	1.140942	7.19822
29.55008	101	0.319638	25.69396
37.11061	102	0.185845	45.07336
42.71118	110	0.841213	10.13613
ZnO:Ag NPs			
2θ(Degree)	(hkl)	d(nm)	FWHM
11.59625	100	4.037181	1.97713
20.80193	002	0.749632	10.77044

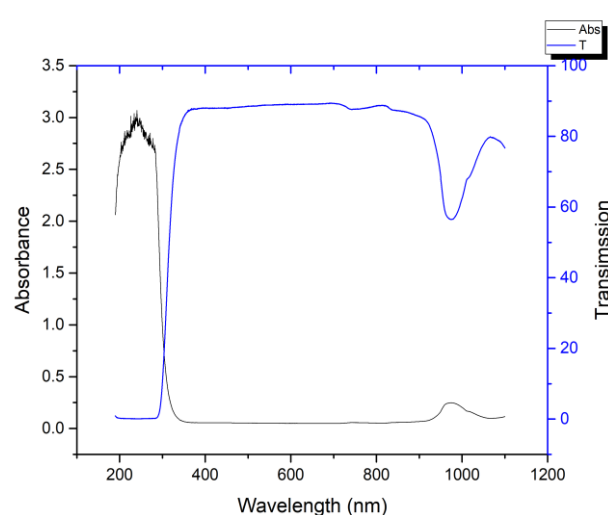
29.13991	101	25.78019	0.31827
31.51086	111	1.191703	6.92387
40.09243	200	0.72901	11.59562
47.92331	102	0.429941	20.21239
47.92331	110	33.32873	0.26074
50.85339	103	7.203885	1.22058

2- UV- Vis analysis

Figure (4 a, b and c) show the transmittance and optical absorption spectrums as function of the wavelength for undoes ZnO, Ag and ZnO doped with Ag NPs, prepared by Pulsed Laser Ablation in Liquid. They were measured by UV-vis spectrophotometer at a wavelength range from 300nm to 900nm. Figure (4 a) shows the produced ZnO nanoparticle suspension, which presents a similar and broad band of ~200 nm. This means that the presence of spherical ZnO nanoparticles with minimal size dispersion, which binds to zinc oxide particles on a nanoscale, reflecting the synthesis was convenient and successful. Figure (4b) shows UV-visible spectroscopy is an important technique to confirm the formation and stability of Ag NP known to exhibit dark brown colours, depending on the density and size of the nanoparticles; colors appear due to surface plasmon resonance (SPR) excitation of AgNPs. Figure (4c) shows the transmittance and absorption spectrum of undead ZnO and ZnO: Ag prepared by ablated Laser.



A



B

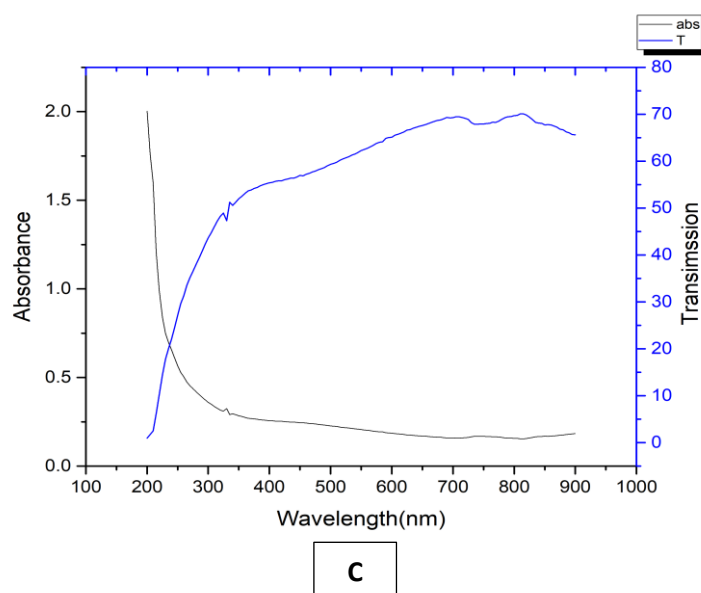
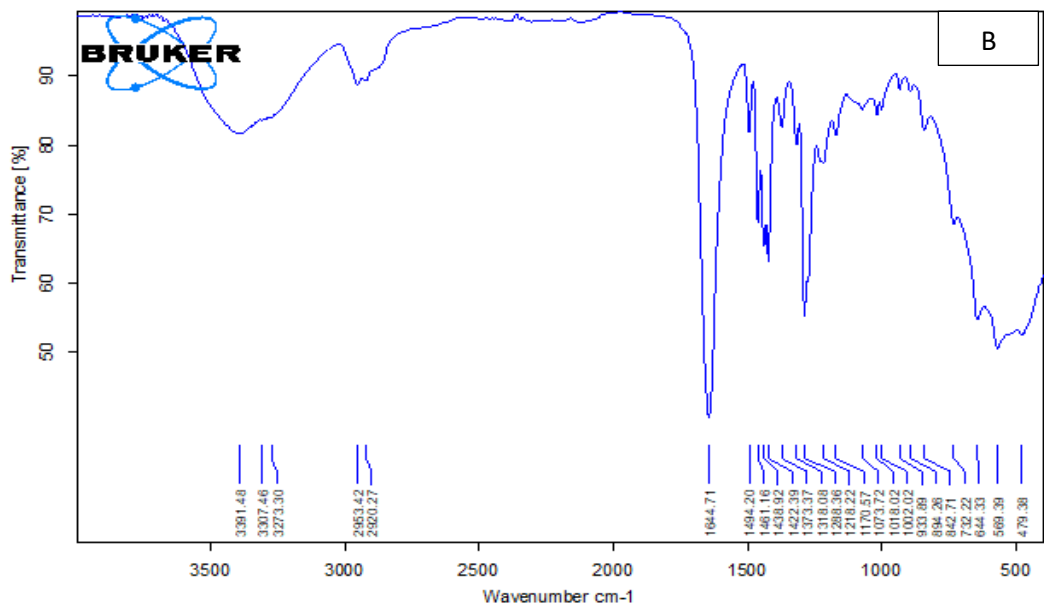
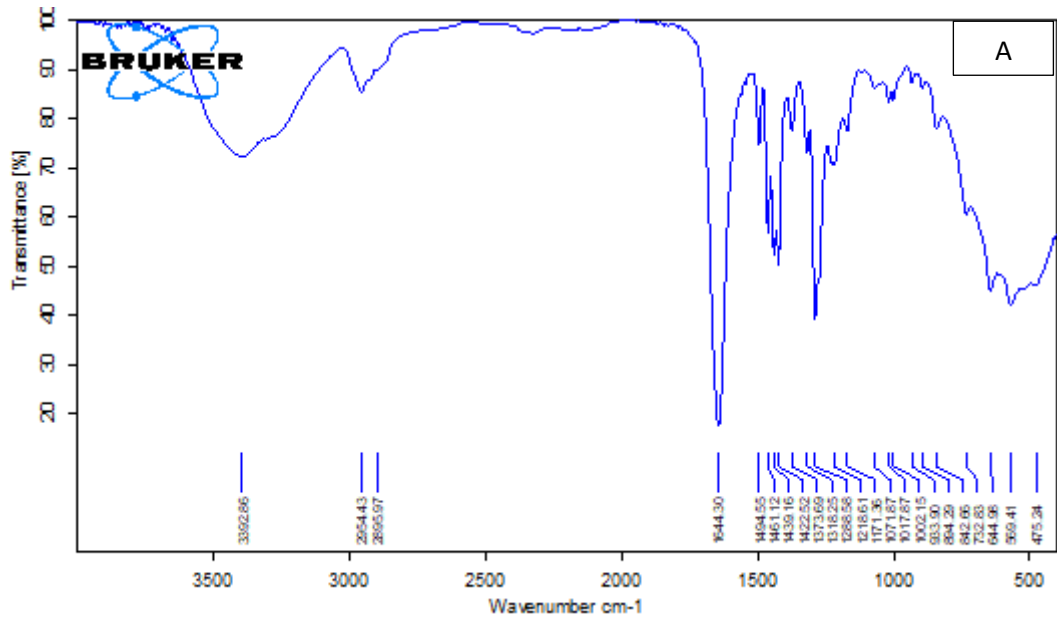


Figure 4: Optical properties of (a)Zinc oxide, (b) sliver and (c) Ag/ZnO nanoparticle.

3- Fourier transformation infrared spectroscopy (FTIR)

Infrared spectroscopy that use Fourier transformation is a crucial tool for observing groups of functions. In order to characterize the various functional groups that contribute to the decrease of the stability of produced ZnO:Ag species, the mentioned technique was used. (A) clarifies ZnO absorption band, the peaks were observed at 1644.30, 2954.43, 2895.97 and 3392.86 cm^{-1} can be ascribed to C=O, C-H and NH, respectively. Figure (5 (B)) exhibits the FT-IR absorption spectrum of Ag nanoparticles. The broad absorption peak at 3391.48 and 3307.46 cm^{-1} can be attributed to the characteristic absorption of NH. The low absorption band located at 1644, 71 cm^{-1} corresponds to C=O stretching modes of vibration. Elongated vibrations is located at 3273.30 cm^{-1} representing amines (OH). The spectra showed the presence of bonds due to O-H (alcohols) stretching at 2965.42 and 2920.27 cm^{-1} and the band which appeared is due to C-H stretching alkane. Figure (5 (C)) displays FTIR absorption spectra of ZnO:Ag NPs . The spectra showed the presence of bonds according to the attached table due to NH (amines) stretching (around 3393.38 cm^{-1}) and the band has appeared at 2964.44 cm^{-1} due to C-H stretching alkane. FTIR spectrum of Ag/ZnO showed absorption band at 1644.13 cm^{-1} , corresponding to the C=O. Strong bands at 493 and 428 cm^{-1} are attributed to the vibrations of elongation and of deformation of vibratory ZnO [29].



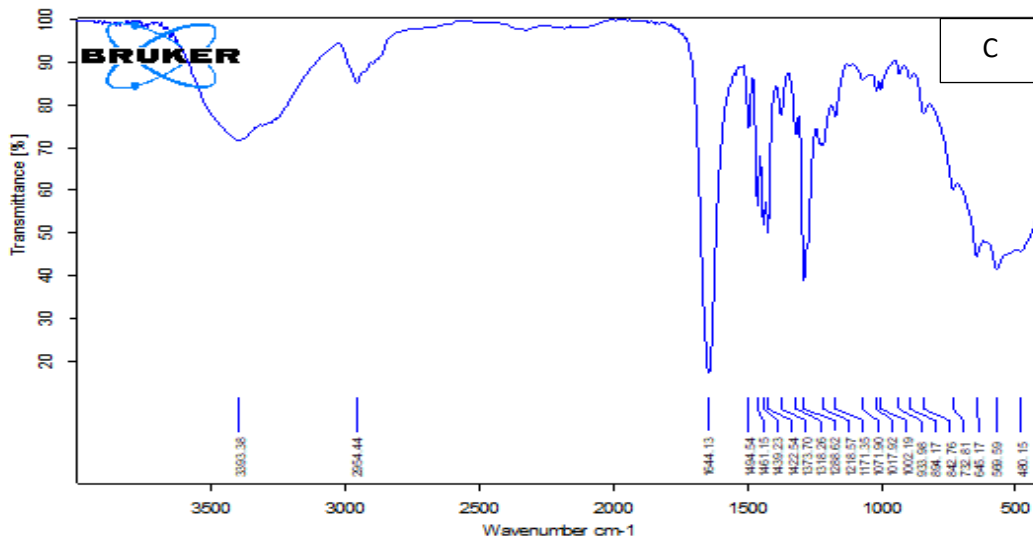


Figure 5: FTIR of (a) Zinc oxide, (b) silver and (c) ZnO:Ag nanoparticles.

4- Transmission Electron Microscope (TEM)

The form and size of synthetic zinc oxide, silver and Zinc oxide: Silver nanoparticles were characterized using TEM analysis. The TEM image (figure (6)) revealed that the ZnO, Ag and ZnO:Ag NPs were spherical in shape, homogeneously distributed and their sizes diverse between 14 and 25 nm.

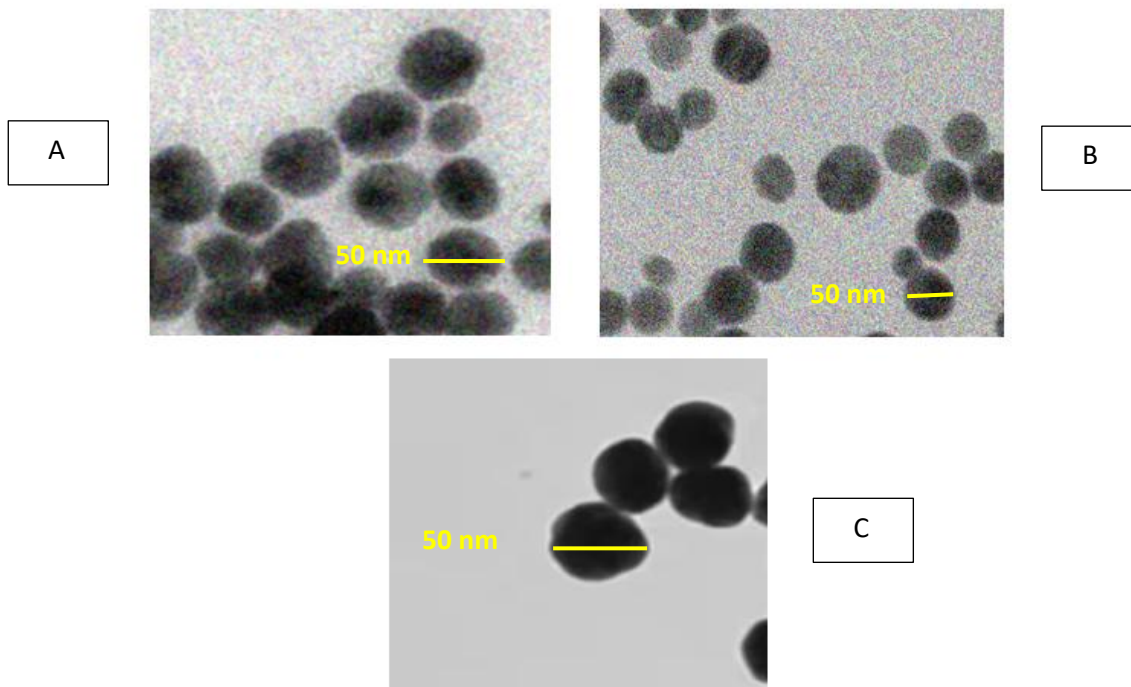


Figure 6: TEM of (a) Zinc oxide, (b) silver and (c) ZnO:Ag nanoparticles.

5- Antibacterial studies

Both (*S. aureus*) and (*E. coli*) with thick peptidoglycan microorganisms have been functioned in antibacterial tests. Researchers have looked at how nanoparticle size affects how effective they are in fighting germs. Researchers have shown that smaller nanoparticle sizes have antimicrobial affected both thick and thin peptidoglycan bacteria, but higher nanoparticle sizes exclusively affect gram negative bacteria. Utilizing the well diffusion approach, antibacterial activity of nanoparticles with lower manufacturing costs than titanium dioxide has been studied. The difference in the zones of suppression for both of the bacteria at assorted calcining temperatures is shown in figure 8. It can be noticed that the thin peptidoglycan bacteria showed to have a higher zone of inhibition than gram negative bacteria. As the calcining temperature is raised, the antibacterial characteristic of the produced nanoparticles diminishes. The zone of inhibition effects of nanoparticles of ZnO stops the development of bacteria by entering or splitting their cell walls through an electrochemical process. When the cell walls are damaged, metabolites seep out and other cell functions halt, stopping the organism from replicating.

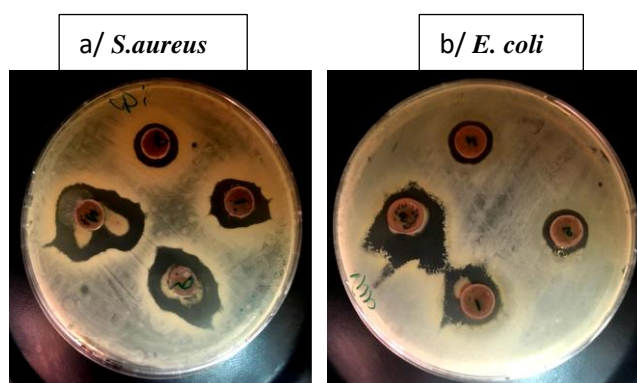


Figure 7: The antibacterial activity of the nanoparticles was investigated using *S.aureus* and *E. coli*
(a) ZnO NPs and (b) ZnO:Ag NPs

Conclusion

In summary, the deposition process of zinc oxide, silver nanoparticles, and zinc oxide: silver particles was carried out using the laser ablation in water method. This method offers advantages such as affordability, speed, and safety, as it eliminates the need for the use of harmful chemicals. The resulting nanoparticles demonstrated a well-defined spherical structure, as confirmed by imaging with EDX and TEM devices. Furthermore, the UV absorption analysis revealed a distinct pattern indicating the nanoparticles' ability to absorb and transmit UV light. Additionally, the FTIR permeability assay was conducted on the zinc oxide nanoparticles. The produced nanoparticles in this

study show promising antibacterial activities against Gram-positive bacteria (*Staphylococcus aureus*) and Gram-negative bacteria (*Escherichia coli*).

References

- [1] SANFELICE, Rafaela C., et al. Hybrid composite material based on polythiophene derivative nanofibers modified with gold nanoparticles for optoelectronics applications. *Journal of Materials Science*, 2017, 52: 1919-1929.
- [2] WANG, Charlie CD, et al. Optical and electrical effects of gold nanoparticles in the active layer of polymer solar cells. *Journal of Materials Chemistry*, 2012, 22.3: 1206-1211.
- [3] JHONG, Hwei-Ru “Molly”, et al. Gold nanoparticles on polymer-wrapped carbon nanotubes: An efficient and selective catalyst for the electroreduction of CO₂. *ChemPhysChem*, 2017, 18.22: 3274-3279.
- [4] TRAN, Tien D., et al. Gold nanoparticles as an outstanding catalyst for the hydrogen evolution reaction. *Chemical Communications*, 2018, 54.27: 3363-3366.
- [5] GHOLINEJAD, Mohammad, et al. Starch functionalized creatine for stabilization of gold nanoparticles: Efficient heterogeneous catalyst for the reduction of nitroarenes. *Inorganica Chimica Acta*, 2019, 495: 118965.
- [6] LI, Bingyu, et al. Colorimetric sensor array based on gold nanoparticles with diverse surface charges for microorganisms identification. *Analytical chemistry*, 2017, 89.20: 10639-10643.
- [7] NIU, Xiaofang, et al. A “turn-on” fluorescence sensor for Pb²⁺ detection based on graphene quantum dots and gold nanoparticles. *Sensors and Actuators B: Chemical*, 2018, 255: 1577-1581.
- [8] CHEN, Ming-Ming, et al. Spatiotemporal imaging of electrocatalytic activity on single 2D gold nanoplates via electrogenerated chemiluminescence microscopy. *Chemical science*, 2019, 10.15: 4141-4147.
- [9] PLAN SANGNIER, Anouchka, et al. Photothermal Therapy: Endosomal Confinement of Gold Nanospheres, Nanorods, and Nanoraspberries Governs Their Photothermal Identity and Is Beneficial for Cancer Cell Therapy (*Adv. Biosys.* 4/2020). *Advanced Biosystems*, 2020, 4.4: 2070042.
- [10] LIU, Hai-Ling, et al. Size-controllable gold nanopores with high SERS activity. *Analytical chemistry*, 2017, 89.19: 10407-10413.
- [11] RODUNER, Emil. Size matters: why nanomaterials are different. *Chemical society reviews*, 2006, 35.7: 583-592.
- [12] EL-SAYED, Ivan H.; HUANG, Xiaohua; EL-SAYED, Mostafa A. Surface plasmon resonance scattering and absorption of anti-EGFR antibody conjugated gold nanoparticles in cancer diagnostics: applications in oral cancer. *Nano letters*, 2005, 5.5: 829-834.
- [13] VEISEH, Omid, et al. Optical and MRI multifunctional nanoprobe for targeting gliomas. *Nano letters*, 2005, 5.6: 1003-1008.
- [14] CHAN, Warren CW; NIE, Shuming. Quantum dot bioconjugates for ultrasensitive nonisotopic detection. *Science*, 1998, 281.5385: 2016-2018.
- [15] PANYAM, Jayanth; LABHASETWAR, Vinod. Biodegradable nanoparticles for drug and gene delivery to cells and tissue. *Advanced drug delivery reviews*, 2003, 55.3: 329-347.
- [16] KOHLER, Nathan, et al. Methotrexate-modified superparamagnetic nanoparticles and their intracellular uptake into human cancer cells. *Langmuir*, 2005, 21.19: 8858-8864.
- [17] RAFFI, M., et al. Antibacterial characterization of silver nanoparticles against *E. coli* ATCC-15224. *Journal of materials science and technology*, 2008, 24.2: 192-196.
- [18] Bindu P and Thomas S 2014 *J. Theor. Appl. Phys.* 8 123–34 ICMLAP 2020 *Journal of Physics: Conference Series* 1795 (2021) 012056 IOP Publishing doi:10.1088/1742-6596/1795/1/012056 8
- [19] Zhang D, Wu X, Han N and Chen Y 2013 *J. Nanopart Res.* 15 1580

- [20] Zhang W, Guo L P, Deng Q W and Li M X 2019 Optik International Journal for Light and Electron Optics 196 1631952
- [21] Kulinich S A, Kondo T, Shimizu Y and Ito T 2013 J. Appl. Phys. 113 033509
- [22] Al-Salman H S, Abdullah M J 2015 Measurement 59 248–57
- [23] Solati E, Dejam L and Dorrnian D 2014 Optics & Laser Technology 58 26–32
- [24] Goto T, Honda M, Kulinich S A, Shimizu Y and Ito T 2015 Japanese Journal of Applied Physics 54 070305
- [25] Moradi M, Solati E, S. Darvishi, and D. Dorrnian 2016 Journal of Cluster Science 27 127– 38
- [26] Guillen G G, Palma M I M, Krishnan B, Avellaneda D, Castillo G A, Das Roy T K and Shaji S 2015 Materials Chemistry and Physics 162 561–70
- [27] M. Idrees, S. Sawant, N. Karodia and A. Rahman," Staphylococcus aureus Biofilm: Morphology, Genetics, Pathogenesis and Treatment Strategies" Int. J. Environ. Res. Public Health, V.18, no. 7602, 2012.
- [28] G. Nagaraju, S. Prashanth, M. Shastri, K. Yathish, C. Anupama, and D. Rangappa, "Electrochemical heavy metal detection, photocatalytic, photoluminescence, biodiesel production and antibacterial activities of Ag–ZnO nanomaterial," Materials Research Bulletin, vol. 94, pp. 54-63, 2017.
- [29] S. K. Sahoo, "Synthesis and characterization of Ag doped ZnO-PVP composite nanofibers by electrospinning method," 2014.